Accepted Manuscript

Facile synthesis of Bi/BiOCl composite with selective photocatalytic properties

Dongling Chen, Min Zhang, Qiuju Lu, Junfang Chen, Bitao Liu, Zhaofeng Wang

PII: S0925-8388(15)30225-5

DOI: 10.1016/j.jallcom.2015.06.113

Reference: JALCOM 34466

To appear in: *Journal of Alloys and Compounds*

Received Date: 23 March 2015

Revised Date: 29 May 2015

Accepted Date: 15 June 2015

Please cite this article as: D. Chen, M. Zhang, Q. Lu, J. Chen, B. Liu, Z. Wang, Facile synthesis of Bi/BiOCl composite with selective photocatalytic properties, Journal of Alloys and Compounds (2015), doi: 10.1016/j.jallcom.2015.06.113.

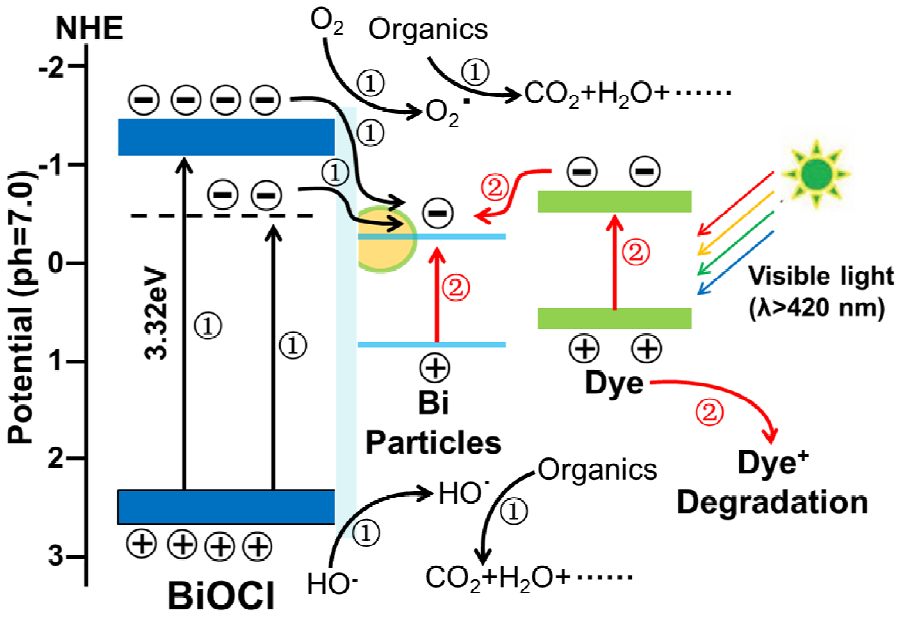

Facile synthesis of Bi/BiOCl composite with selective photocatalytic properties

Dongling Chen[1], Min Zhang[1], Qiuju Lu[1], Junfang Chen[1], Bitao Liu[1]*, Zhaofeng Wang[2]*

[1] Research institute for new material technology, Department of Research Center for Materials Interdisciplinary Science, Chongqing University of Arts and Science, Chongqing 402160, PR. China

[2] Department of Chemical & Biomolecular Engineering and Polymer Program, Institute of Materials Science, University of Connecticut, Storrs, Connecticut 06269, United States

*Corresponding authors

Email: liubitao007@163.com (B. Liu); zhaofeng.wang@uconn.edu (Z. Wang)

Tel.: +86-023-49891752

Abstract:

This paper presents a novel and facile method to fabricate Bi/BiOCl composites with dominant (001) facets in situ via a microwave reduction route. Different characterization techniques, including X-ray diffraction (XRD), field-emission scanning electron microscopy (FE-SEM), transmission scanning electron microscopy (TEM), UV-vis diffuse reflectance spectrometry (DRS), X-ray photoelectron spectroscopy (XPS), electron spin resonance spectroscopy (ESR), cathodoluminescence spectrum (CL), and lifetime, have been employed to investigate the structure, optical and electrical properties of the Bi/BiOCl composites. The experimental results show that the introduction of Bi particles can efficiently enhance the photocatalytic performance of BiOCl for the degradation of several dyes under ultraviolet (UV) light irradiation, especially for negative charged methyl orange (MO). Unlike the UV photocatalytic performance, such Bi/BiOCl composite shows higher degradation efficiency towards rhodamine B (RhB) than MO and methylene blue (MB) under visible light irradiation. This special photocatalytic performance can be ascribed to the synergistic effect between oxygen vacancies and Bi particles. This work provides new insights about the photodegradation mechanisms of MO, MB and RhB under UV and visible light irradiation, which would be helpful to guide the selection of an appropriate catalyst for other pollutants.

Key words : Photocatalyst; Composites; Semiconductors; BiOCl

1. Introduction:

The decontamination of waste air and water through photocatalytic reactions, e.g., semiconductor photocatalysis, has drawn much attention during recent years[1-3]. Photocatalysis has been considered as one of the most promising approaches to solve the pollution problems. Bismuth-based oxides are suggested to be good candidates because of their chemical and thermal stability, nontoxicity, and photocatalytic activity [4-7]. Among them, bismuth oxychloride (BiOCl) attracts particular interest, which exhibits higher photocatalytic activity than that of TiO_2 in UV light region. The excellent photocatalytic performance of BiOCl could be attributed to its characteristic layered structure, optical property, as well as higher stability [8, 9]. Since the recombination rate of electron and hole in semiconductor photocatalysts is crucial to the photocatalytic efficiency, it is highly desirable to develop an efficient way to improve the separation of the photo-induced electron–hole pairs in BiOCl[10-12].

It is well known that molecular oxygen is green and low-cost oxidant, and photocatalysis will activate molecular oxygen when electrons are generated on the surface of semiconductor photocatalysts. The surface would be the key point, which not only produces reactive oxygen species (ROS) like ·OH, $\cdot O^{2-}$ and H_2O_2, but also inhibits the recombination of photo-induced electron/hole pairs [13-19]. For example, it is reported that O_2 would adsorb onto the oxygen vacancies of TiO_2 surfaces and be further converted into $\cdot O^{2-}$ or O_2^{2-}, which act as a recombination center of photo-induced electron/hole pairs and therefore enhance its photocatalytic activity [13, 17, 19-21]. It is interesting and shows an inspiration to modify BiOCl.

Actually, the layered structure feature of BiOCl endows itself internal static electric

fields that can promote the effective separation of the photo-induced electron–hole pairs [22, 23]. Moreover, density functional theory (DFT) calculations by Zhou et al. showed that oxygen vacancies were stable and energetically favorable within BiOCl surface [24]. Aimed at this, some experimental work has also been carried out. For example, Ye et al. [25] reported that black BiOCl was prepared from white BiOCl by UV light irradiation; Yan et al. [26] synthesized oxygen vacancies contained black BiOCl by Fe reduction; Hu et al. [27] prepared oxygen vacancies contained Bi/BiOCl composites by KBH_4 reduction. All of the above work showed enhanced photocatalytic activities. However, for an ideal catalyst, it should be multifunctional under various environmental conditions. To date, investigations on various organic molecule dyes have not been carried out.

Herein, we prepared oxygen vacancies contained Bi/BiOCl under microwave irradiation, and examined its adsorption and photocatalytic performance for the degradation of dyes with different molecular structures (MO, MB and RhB). The results provide a clearly understanding of the degradation mechanisms of oxygen vacancies contained BiOCl, which will be useful for the development of catalysts in water treatment facilities and environmental remediation projects.

2. Experimental section

2.1 Preparation of BiOCl

Typically, 1.2148 g $Bi(NO_3)\cdot 5H_2O$ and 1.1378 g mannitol were dissolved in 20 mL deionized water, after which 10 mL saturated NaCl solution were added. The mixture was then transferred to a 50 mL Teflon-lined autoclave, and maintained at 150 ^oC for 4 h. After cooling down, the product was washed and dried.

2.2 Preparation of Bi/BiOCl composites

For the Bi/BiOCl composites, 1 g sample was first dispersed in 100 mL deionized water. Then, the mixture was treated at 140 ^{o}C for 5-180 min by reflux under microwave irradiation in a microwave reactor (WF-3000, PreeKem Scientific Instruments Co., Ltd., China) operating at a power of 900W. The obtained sample was finally washed and dried. The samples were numbered by its microwave treated time, e.g., sample treated with microwave for 5 min was labeled as 5 MT-BiOCl.

2.3 Characterization

The morphology and microstructure of the samples were observed by field emission scanning electron microscope (FESEM, Hitachi, SU-8020), transmission electron micros-copy (TEM), highly resolution transmission electron micros-copy (HRTEM), selected area electron diffraction (SAED). Crystal phase of the obtained materials were determined by powder X-ray diffraction (XRD, Rigaku D/MAX-2400 X-ray diffract meter with Ni-filtered Cu-Ka irradiation λ=1.54056 Å). UV-vis diffuse reflectance spectra were recorded on a Hitachi UV-3900 spectrophotometer with an integrating sphere, and $BaSO_4$ was used as the reference. X-ray photoelectron spectroscopy (XPS, PHI-5702, Physical Electronics) was performed using a monochromated Al K_α irradiation. Peak deconvolution and quantification of elements were accomplished using Origin 8.0. Low-voltage CL spectra were obtained using a modified Mp-Micro-S instrument. Fluorescence lifetimes were measured on a Perkin-Elmer LS 50B spectrofluorimeter by the time-correlated single photon counting method.

2.4 Catalyst activity test

The liquid-phase photo-degradation of different dyes (MO, MB and RhB) was carried

out in a quartz tube under the irradiation of UV light and visible light, respectively. In a typical process for degradation of dyes under the UV irradiation, 0.2 g catalyst was suspended in 500 mL of 20 ppm dyes solution. Before irradiation, the suspensions were stirred in the dark for 0.5 h to ensure the establishment of adsorption desorption equilibrium. Under ambient conditions and stirring, the quartz tube was exposed to the UV irradiation produced by a 500 W Xe arc lamp equipped with a band-pass light filter (365 ± 15 nm). 3 mL sample solution was taken at a certain time interval during the experiment and centrifuged to remove the catalyst completely. The solution was analyzed on a Varian UV–vis spectrophotometer (Cary-50, Varian Co.). The percentage of degradation is reported as C/C_0. Here, C is the absorption of dyes solution at each irradiated time interval of the main peak of the adsorption spectrum, while C_0 is the absorption of the initial concentration when the adsorption desorption equilibrium is reached. For the visible light photocatalytic degradation of dyes, a UV cut off filter (λ> 420 nm) was used while the other experimental conditions are the same as that of the above-mentioned degradation of dyes under the UV light irradiation.

3. Results and discussions

SEM images of pure BiOCl and the microwave treated BiOCl (MT-BiOCl) powders are shown in Fig. 1. It is clearly observed that these products are composed of a large amount of well-defined square-like nanosheets, which are 100–200 nm in width and 20–25 nm in thickness. As suggested in previous researches [22-25], the indices of crystal face of the square facets should be (001). For the MT-BiOCl composites (Fig. 1c, d), the morphology is almost same as the pure BiOCl. Obviously, the microwave treatment of BiOCl did not significantly affect their morphologies in relatively macro perspective. The

detailed microstructure is shown in Fig. 2.

As shown in the TEM/HRTEM images of Fig. 2, it is also found that the BiOCl nanoplates are 100–200 nm in width and 20-25 nm in thickness, which is in good consistent with the SEM observations. For the pure BiOCl, the surface is smooth and clean (as shown in Fig. 2c), which exhibits clear lattice fringes of the side face of a single BiOCl nanosheet with d-spacing of 0.734 nm (Fig. 2e), corresponding to the (001) lattice plane. This suggests that the BiOCl nanosheets are well-crystallized and possess a high order of crystallinity. The SAED pattern also confirms the single-crystal feature of the free standing crystal and its unique pattern of diffraction spots could be readily indexed to (110) and (200) planes, indicating that the preponderant growth direction of the obtained samples is [001] orientation. For the MT-BiOCl, it is found that there are some particles adhered on the surface as shown in Fig. 2d and f. As the lattice fringes with d-spacing of 0.328 nm revealed by the HRTEM corresponds to the (012) lattice plane of Bi, these particles are confirmed to be Bi, which agrees well with previous reports [26, 27].

Figure 3 shows typical XRD patterns of the different samples. The diffraction peaks of pure BiOCl are in good accordance with the standard card (JCPDS 06–0249) without appearing any impurity peaks, suggesting it is of tetragonal structure. It can be seen that the diffraction peak intensity of the (001) plane in these spectra is obviously stronger than that of the (110) plane. It indicates that the crystal exhibits special anisotropic growth along the [001] direction, which agrees well with the TEM results. However, after BiOCl undergoing the microwave treatment (Fig. 3b-g), the (001) peak is greatly decreased along with the increased microwave irradiation time, suggesting there is a change on the microstructure.

On the basis of the above results, we tested the photocatalytic activity of these samples for the photodegradation of MO, MB and RhB under UV and visible light irradiation. It can be seen that all samples show a quick degradation rate under UV light irradiation. It degrades MO faster than MB and RhB. For the 30 MT-BiOCl, it can degrade almost all the MO in 6 min, faster than that of 76% and 68% for MB and RhB. Interestingly, for MB and RhB, the dark absorption properties are enhanced with the microwave treatment time increased. For the 30 MT-BiOCl sample, it can absorb 30% of MB and 20% of RhB in 30 min, which is much higher than the 7% of MB and 8% of RhB for the untreated sample. However, there is almost no change for the dark absorption properties of MO by increasing the treat time. Such phenomena could be attributed to the electrostatic interactions between the surface of catalyst and the dye with different structures as shown in Fig. 5. It is well accepted that RhB and MB molecules would form positively charged cations in aqueous solution and thus could be adsorbed on the surface of BiOCl via electrostatic interactions. In contrast, MO molecules would form anions in solution, preventing the above absorption behavior. With the increase of the microwave irradiation time, more Bi particles will be generated, and the surface of BiOCl becomes more negatively charged. As a result, the absorption of positively charged RhB and MB molecules would be enhanced with the microwave irradiation time increased.

When the dyes are tested under visible light irradiation, the degradation properties are significant different. It only degrades 23% of MO and 5% of MB in 200 min, both of which are much slower than 100% of RhB. It is obviously found that the MT-BiOCl exhibits better photocatalyst properties than the untreated sample. In addition, the MT-BiOCl shows a very good photocatalytic activity toward RhB under visible light

irradiation, implying that the dye degradation occurs via a dye sensitized mechanism [28, 29]. In addition to the different molecular structures, the changed surface microstructure should also be responsible for this phenomenon. To better understand the relationship between surface microstructure and photocatalytic activity, more effective detection methods were used.

XPS is a powerful tool to identify the surface element states [30-32]. XPS spectra were recorded to confirm the elemental composition of the BiOCl and MT-BiOCl as shown in Fig. 6. The high-resolution XPS spectra of Bi 4f are shown in Fig. 6a. Two peaks with binding energies of 158.8 eV and 164.2 eV can be observed in the spectrum of the BiOCl nanosheets, which can be ascribed to the binding energies of Bi^{3+} $4f^{7/2}$ and Bi^{3+} $4f^{5/2}$, respectively. The result suggests that there are only triple charged Bi ions in the untreated BiOCl. However, for the MT-BiOCl, it can be seen that two additional peaks with relative low intensity appear at 162.4 eV and 157.0 eV, which can be ascribed to metallic Bi [26, 27]. Therefore, after a microwave treatment, the sample contains both BiOCl and metallic Bi.

The XPS spectrum of O 1s is presented in Fig. 6b, which displays two peaks at 530.1 eV and 532.9 eV, respectively. It is confirmed that low-BE peak at 530.1 eV could be assigned to the normal O in the crystal structure of BiOCl, while the high-BE peak at 532.9 eV could be attributed to the oxygen vacancies [33, 34]. This result is consistent with the reported work, which would be beneficial to the photocatalytic activity [24, 25]. Therefore, these oxygen vacancies play roles on gathering positive charges on the surface, leading to the preferential absorption of the negative dye molecules (MO), which well explains the photocatalytic results under UV light irradiation.

The EPR technique is an effective and common method to detect defects in materials. Here, the EPR technique was applied to detect oxygen vacancies. Fig. 7 shows the EPR spectra of pure BiOCl and MT-BiOCl. There is no EPR signal from the pure BiOCl, which means there are few oxygen vacancies, hard to be detected by EPR [24, 25]. On the contrary, a remarkable EPR signal from MT-BiOCl is observed, and the peak at g = 2.001 is the characteristic signal of oxygen vacancies [35, 36]. It indicates that the microwave treatment could largely modify the surface microstructure and induce the formation of oxygen vacancies like the UV irradiation in previous work [25].

UV-vis spectroscopy has been proved to be an effective optical characterization method for understanding the electronic structure in semiconductors. As shown in Fig. 8, the optical properties of pure BiOCl and MT-BiOCl were measured by UV-vis diffuse reflectance spectroscopy. It reveals that the absorbance of BiOCl in the visible region is negligible. Unlike pure BiOCl, the MT-BiOCl exhibits a continuous absorption band in the range of 400–700 nm, which is in accordance with the color change of the samples. Interestingly, the MT-BiOCl shows stronger absorption intensity in the UV region than that of pure BiOCl, demonstrating its higher photocatalytic activity under UV light irradiation. The band gaps of BiOCl and MT-BiOCl estimated by the Kubelka–Munk function are approximately 3.32 eV and 3.24 eV, respectively. The band gap narrowing of the BiOCl semiconductor is ascribed to the modification of surface microstructure by Bi particles and oxygen vacancies, following the color change from white to black as shown in Fig. 8.

For a deep investigation, the CL spectra were obtained. As shown in Fig. 9, the CL spectrum of pure BiOCl exhibits an asymmetric distribution, and the intensity is much

higher than that of the MT-BiOCl. Using Gaussian decomposition, the spectrum can be divided into two main peaks at 385 and 475 nm, respectively. Obviously, the peak at 385 nm (~3.22eV) is the bandgap emission, while the emission at 475 nm should be ascribed to the surface oxygen vacancies which can be easily formed in the high energy (001) facets [24, 25]. This is consistent with the results in previous work [24, 25].

However, when BiOCl is treated by microwave (MT-BiOCl), the CL spectrum is very different. First of all, the emission intensity is decreased to 38.9% of the pure BiOCl; secondly, the emissions of the bandgap and oxygen vacancies shift to 414 and 485 nm, respectively; thirdly, a new peak appears at 586 nm. The emission peak shift of bandgap and oxygen vacancies could be attributed to the Schottky barrier between BiOCl and Bi particles, while the new CL peak at 586 nm should be originated from the Bi particles. The energy barrier would make the conduction band of BiOCl at the junction area bending to a lower energy level, and the band gap is slightly decreased. Consequently, the CL spectra would shift to a lower energy. This implies these Bi particles would play an important role in photocatalysis.

The recombination of electron–hole pairs is also characterized by the lifetime of carriers, which can indirectly imply the electrons transfer in semiconductors [37]. It can be reflected by the decays of PL transition centered on 480 nm excited at 350 nm as shown in Fig. 10. The PL lifetime calculated by the exponential analysis is also presented. The PL lifetimes of BiOCl and MT-BiOCl are determined to be ca. 1.1 and 2.04 ns, respectively. The longer PL lifetime of MT-BiOCl suggests its lower electron–hole recombination rate, which implies the more efficient trap ability of the oxygen vacancies states.

Based on the above investigations, a schematic illustration is proposed as shown in Fig. 11. When irradiated by UV light, electrons will be excited from valance band to conduction band of BiOCl. Because of the newly formed oxygen vacancies, most of the excited electrons will be trapped by the oxygen vacancies states. Due to the potential differences among conduction band, oxygen vacancies states and the adhered Bi particles, the excited electrons would be transferred to Bi particles. The oxygen vacancies would make this transformation more easily as process ① exhibited. This would activate the catalyst and the hole in the valance band can participate in oxidizing reaction. Additionally, Bi particles also would act as a semiconductor [38]. The electron band of the Bi particles is at about -0.28 eV as calculated by the work function of metallic bismuth of 4.22 eV, which is more positive than -1.1 eV for the conduction band of BiOCl [27]. Therefore, the space charge layer at the Bi-BiOCl junctions could accelerate the electrons transfer from BiOCl to Bi particles, efficiently decreasing the recombination rate and thus enhance the photocatalytic performance [27].

For the visible light irradiation, the dye degradation is achieved via a dye sensitized mechanism. The excited dye can transfer electrons to the electron band of Bi particles or other semiconductors to generate reactive oxygen species (ROSs) as process ②. The dye acts as both a sensitizer and a pollutant [39-41]. In the dye-sensitized mechanism, a good charge transfer followed by separation is an important step. The LUMO of dyes and the CB of the catalyst is another key factors for the higher charge transfer. A good interfacial wave function mixing (or a well-aligned energy level) promotes the charge transfer rate. Obviously, this decomposed process depends on the structures of the organic dyes. As

reported, an efficient N-dealkylation (preceded by radical cation formation) was observed with RhB, but not MB [42]. The injection of an electron from excited dye and its transfer to a mild oxidant proceeds at separate positions on the semiconductor surface, and thus $RhB^{+}\cdot$-e_{cond}^{-} recombination is effectively prevented [42]. Additionally, for the dyes can hardly excited by visible light, such as MO and MB, their degradation should due to the oxidation of the actively species as process ① exhibited. As a result, dyes with different structures show various decomposition efficiency under visible light irradiation as shown in Fig. 4.

4. Conclusion

This work presents a novel and facile method to fabricate Bi/BiOCl composites. The structure, optical and electrical properties of the Bi/BiOCl composite were investigated in detail. The results show that the properties of the samples, including their optical and electrical properties, can be tuned by the modification of Bi particles. It is found that the Bi particles can efficiently enhance the photocatalytic performance of BiOCl for the degradation of different dyes under UV light irradiation. It can degrade almost all the MO in 6 min, faster than that of MB and RhB. This should be ascribed to the co-work between the oxygen vacancies and Bi particles, which can efficiently separate the electron-hole recombination via the oxygen vacancies states. For the photocatalytic performance under visible light irradiation, it can degrade much more RhB than MO and MB. Compared with the 100% of RhB, it only degrades 23% of MO and 5% of MB in 200 min, due to the molecular structures. The results provide a new insight on the photodegradation mechanism of different dyes under UV and visible light irradiation, which will be helpful to select appropriate catalysts for pollutants.

Acknowledgement

This study is supported by Chongqing Natural Science Foundation (cstc2013jcyjA20023), Scientific and Technological Research Program of Chongqing Municipal Education Commission (KJ1401111), Foundation of Chongqing University of Arts and Sciences (Z2013CJ01 and R2013CJ05).

Reference

[1] H. G. Yang, C. H. Sun, S. Z. Qiao, J. Zou, G. Liu, S. C. Smith, H. M. Cheng and G.Q. Lu, Anatase TiO_2 single crystals with a large percentage of reactive facets, Nature, 453 (2008) 638-41.

[2] B. T. Liu, Y. J. Huang, Y. Wen, L. J. Du, W. Zeng, Y. R. Shi, F. Zhang, G. Zhu, X. X. Xu and Y. H. Wang, Highly dispersive {001} facets-exposed nanocrystalline TiO_2 on high quality graphene as a high performance photocatalyst, J. Mater. Chem, 22 (2012) 7484-7491.

[3] B. T. Liu, L. L. Tian and Y. H. Wang, One-Pot Solvothermal Synthesis of ZnSe·xN2H4/GS and ZnSe/N-GS and Enhanced Visible-Light Photocatalysis, ACS Appl. Mater. Interfaces, 5 (2013) 8414-8422.

[4] H. B. Fu, C. S. Pan, W. Q. Yao, Y. F. Zhu, Visible-Light-Induced Degradation of Rhodamine B by Nanosized Bi_2WO_6, J. Phys. Chem. B, 109 (2005) 22432−22439.

[5] M. W. Stoltzfus, P. M. Woodward, R. Seshadri, J.-H. Klepeis, B. Bursten, Structure and Bonding in $SnWO_4$, $PbWO_4$, and $BiVO_4$: Lone Pairs vs Inert Pairs, Inorg. Chem., 46 (2007) 3839−3850.

[6] L. S. Zhang, W. Z. Wang, J. O. Yang, Z. G. Chen, W. Q. Zhang, L. Zhou, S. W. Liu, Sonochemical Synthesis of Nanocrystallite Bi_2O_3 as a Visible-Light-Driven Photocatalyst,

Appl. Catal. A, 308 (2006) 105−110.

[7] J. B. Liu, H. Wang, S. Wang, H. Yan, Hydrothermal Preparation of $BiVO_4$ Powders, Mater. Sci. Eng. B, 104 (2003) 36−39.

[8] Y. Lei, G. Wang, S. Song, W. Fan and H. Zhang, Synthesis, characterization and assembly of BiOCl nanostructure and their photocatalytic properties, CrystEngComm, 11 (2009) 1857-1862.

[9] X. Zhang, Z. Ai, F. Jia and L. Zhang, Generalized One-Pot Synthesis, Characterization, and Photocatalytic Activity of Hierarchical BiOX (X = Cl, Br, I) Nanoplate Microspheres, J. Phys. Chem. C, 112 (2008) 747-753.

[10] T. Berger, M. Sterrer, O. Diwald, E. Knozinger, D. Panayotov, T. L. Thompson and J. T. Yates, Light-Induced Charge Separation in Anatase TiO_2 Particles, J. Phys. Chem. B, 109 (2005) 6061–6068.

[11] W. Dai, X. Wang, P. Liu, Y. Xu, G. Li and X. Fu, Effects of Electron Transfer between TiO_2 Films and Conducting Substrates on the Photocatalytic Oxidation of Organic Pollutants, J. Phys. Chem. B, 110 (2006) 13470–13476.

[12] X. H. Wang, J. G. Li, H. Kamiyama, Y. Moriyoshi and T. Ishigaki, Wavelength-Sensitive Photocatalytic Degradation of Methyl Orange in Aqueous Suspension over Iron(III)-doped TiO_2 Nanopowders under UV and Visible Light Irradiation, J. Phys. Chem. B, 110 (2006) 6804–6809.

[13] A. L. Linsebigler, G. Q. Lu, J. T. Yates, Photocatalysis on TiO_2 Surfaces: Principles, Mechanisms, and Selected Results, Chem. Rev., 95 (1995) 735-758.

[14] T. Wang, X.Yan, S. Zhao, B. Lin, C. Xue, G. Yang, S. Ding, B. Yang, C. Ma, G. Yang, G. Yang, A facile one-step synthesis of three-dimensionally ordered macroporous

N-doped TiO2 with ethanediamine as the nitrogen source, J. Mater. Chem. A, 2(2014), 15611,

[15] C. Xue, T. Wang, G. Yang, B. Yang, S. Ding, A facile strategy for the synthesis of hierarchical TiO2/CdS hollow sphere heterostructures with excellent visible light activity, J. Mater. Chem. A, 2(2014), 7674.

[16] C. Xue, J. Xia, T. Wang, S. Zhao, G. Yang, B. Yang, Y. Dai, G. Yang, A facile and efficient solvothermal fabrication of three-dimensionally hierarchical BiOBr microspheres with exceptional photocatalytic activity, Materials Letters, 133(2014), 274.

[17] N. G. Petrik, G. A. Kimmel, Oxygen Photochemistry on TiO_2(110): Recyclable, Photoactive Oxygen Produced by Annealing Adsorbed O_2, J. Phys. Chem. Lett., 2 (2011) 2790.

[18] Z. T. Wang, Y. G. Du, Z. Dohnalek, I. Lyubinetsky, Direct Observation of Site-Specific Molecular Chemisorption of O_2 on TiO_2(110), J. Phys. Chem. Lett., 1 (2010) 3524-3529.

[19] U. Aschauer, J. Chen, A. Selloni, Peroxide and superoxide states of adsorbed O_2 on anatase TiO_2 (101) with subsurface defects, Phys. Chem. Chem. Phys., 12 (2010) 12956.

[20] G. Yang, Z. Yan, T. Xiao, B. Yang, Low-temperature synthesis of alkalis doped TiO2 photocatalysts and their photocatalytic performance for degradation of methyl orange, Journal of Alloys and Compounds, 580(2013), 15.

[21] M. Setvín, U. Aschauer, P. Scheiber, Y. F. Li, W. Y. Hou, M. Schmid, A. Selloni, U. Diebold, Reaction of O_2 with Subsurface Oxygen Vacancies on TiO_2 Anatase (101), Science, 341 (2013) 988.

[22] J. Jiang, X. Zhang, P. B. Sun and L. Z. Zhang, ZnO/BiOI Heterostructures: Photoinduced Charge-Transfer Property and Enhanced Visible-Light Photocatalytic Activity, J. Phys. Chem. C, 115 (2011) 20555.

[23] S. Wu , C. Wang, Y. Cui , W. Hao, T. Wang and P. Brault, BiOCl nano/microstructures on substrates: Synthesis and photocatalytic properties, Appl. Catal. B, 68 (2006) 125.

[24] H. J. Zhang, L. Liu and Z. Zhou, Towards better photocatalysts: first-principles studies of the alloying effects on the photocatalytic activities of bismuth oxyhalides under visible light, Phys. Chem. Chem. Phys., 14 (2012) 1286.

[25] L. Ye, K. Deng, F. Xu, L. Tian, T. Peng, L. Zan. Increasing visible-light absorption for photocatalysis with black BiOCl, Phys Chem Chem Phys 14 (2012) 82–85.

[26] Y. Li, C. Li, X. Sun, Z. Zhang, Z. Peng, J. Zhang and J. Zhao, Preparation of black BiOCl with visible light photocatalytic activity by Fe reduction, Materials Letters, 116 (2014) 98–100.

[27] J. Hu, G. Xu, J. Wang, J. Lv, X. Zhang, Z. Zheng, T. Xie and Y. Wu, Photocatalytic properties of Bi/BiOCl heterojunctions synthesized using an in situ reduction method, New J. Chem., 38 (2014) 4913-4921.

[28] B. Subash, B. Krishnakumar, M. Swaminathan and M. Shanthi, Highly Efficient, Solar Active, and Reusable Photocatalyst: Zr-Loaded Ag–ZnO for Reactive Red 120 Dye Degradation with Synergistic Effect and Dye-Sensitized Mechanism, Langmuir, 29 (2013) 939–949.

[29] Y. F. Fang, W. H. Ma, Y. P. Huang and G. W. Cheng, Exploring the Reactivity of Multicomponent Photocatalysts: Insight into the Complex Valence Band of BiOBr,

Chem.–Eur. J., 19 (2013) 3224–3229.

[30] Y. Wang, Y. Y. Shao, D. W. Matson, J. H. Li, Y. H. Lin, Nitrogen-Doped Graphene and Its Application in Electrochemical Biosensing, ACS Nano, 4 (2010) 1790-1798.

[31] A. H. Gröschel, F. H. Schacher, H. Schmalz, O. V. Borisov, E. B. Zhulina, A. Walther and A. H. E. Müller, Precise hierarchical self-assembly of multicompartment micelles, Nat. Commun., 3 (2012), 1643.

[32] Z.Wang, J.Wanga, Z. Li, P. Gong, X. Liu, L. Zhang, J. Ren, H. Wang, S. Yang, Synthesis of fluorinated graphene with tunable degree of fluorination, Carbon, 50(2012), 5403.

[33] X. Chen, L. Liu, P. Y. Yu and S. S. Mao, Increasing Solar Absorption for Photocatalysis with Black Hydrogenated Titanium Dioxide Nanocrystals, Science, 331 (2011) 746–750.

[34] X. Q. Wei, B. Y. Man, M. Liu, C. S. Xue, H. Z. Zhuang and C. Yang, Blue luminescent centers and microstructural evaluation by XPS and Raman in ZnO thin films annealed in vacuum, N_2 and O_2, Phys. B, 388 (2007) 145–152.

[35] C. Feng, Y. Wang, Z. Jin, J. Zhang, S. Zhang, Z. Wu and Z. Zhang, Photoactive centers responsible for visible-light photoactivity of N-doped TiO_2, New J. Chem., 32 (2008) 1038–1047;

[36] D. Pan, G. Xu, L. Lv, Y. Yong, X. Wang, J. Wan and G. Wang, Effects of oxygen vacancy location on the electronic structure and spin density of Co-doped rutile TiO_2 dilute magnetic semiconductors, Phys. Rev. Lett., 89 (2006) 082510.

[37] C. Pan, J. Xu, Y. Wang, D. Li, Y. Zhu, Dramatic Activity of $C_3N_4/BiPO_4$ Photocatalyst with Core/Shell Structure Formed by Self-Assembly, Adv. Funct. Mater.,

22 (2012) 1518.

[38] Y. W. Wang, J. S. Kim, G. H. Kim and K. S. Kim, Quantum size effects in the volume plasmon excitation of bismuth nanoparticles investigated by electron energy loss spectroscopy, Appl. Phys.Lett., 88 (2006) 143106.

[39] D. Chatterjee, S. Dasgupta, Visible light induced photocatalytic degradation of organic pollutants, J. Photochem. Photobiol C, 6 (2005) 186−205.

[40] D. Zhao, C. Chen, Y. Wang, W. Ma, J. Zhao, T. Rajh, L. Zang, Enhanced Photocatalytic Degradation of Dye Pollutants under Visible Irradiation on Al(III)-Modified TiO2: Structure, Interaction, and Interfacial Electron Transfer, Environ. Sci. Technol., 42 (2008) 308−314.

[41] P. F. Ji, J. L. Zhang, F. Chen, M. Anpo, A Highly Efficient and Stable Visible-Light Plasmonic Photocatalyst Ag-AgCl/CeO_2, Appl. Catal., B, 85 (2009) 148−154.

[42] T. Takirawa, T. Watanabe, and K. Honda, Photocatalysis through excitation of adsorbates. 2. A comparative study of Rhodamine B and methylene blue on cadmium sulfide, Journal of Physical Chemistry, 82 (1978) 1391.

Figure caption

Figure 1. SEM micrographs of pure BiOCl (a, b) and MT-BiOCl (c, d).

Figure 2. TEM/HRTEM images of pure BiOCl (a, c, e) and MT- BiOCl (b, d, f).

Figure 3. Typical XRD patterns pure BiOCl (a) and seriouse MT- BiOCl (b-f).

Figure 4. Liquid-phase photocatalytic degradation of MO (a, b), MB(c, d) and Rhb (e, f) under UV light and visible light irradiation.

Figure 5. The molecular structures of the three different dyes.

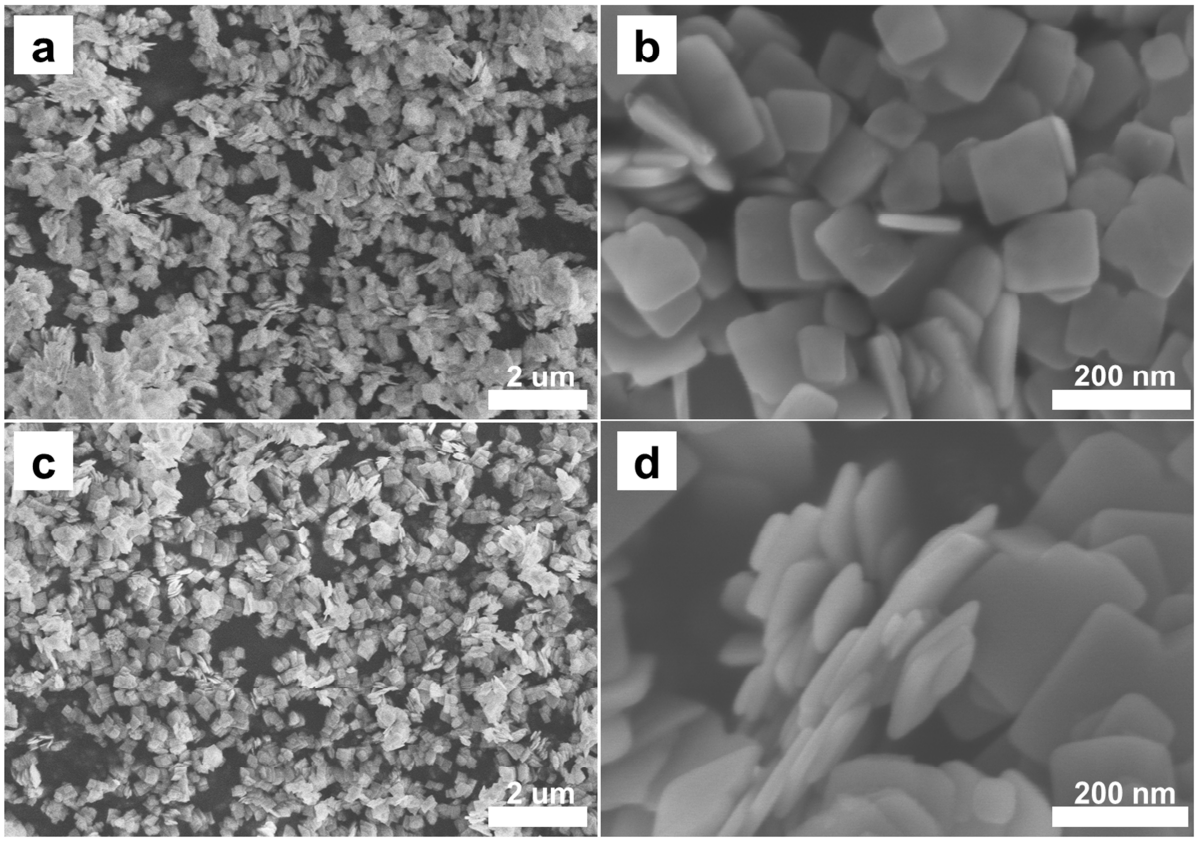

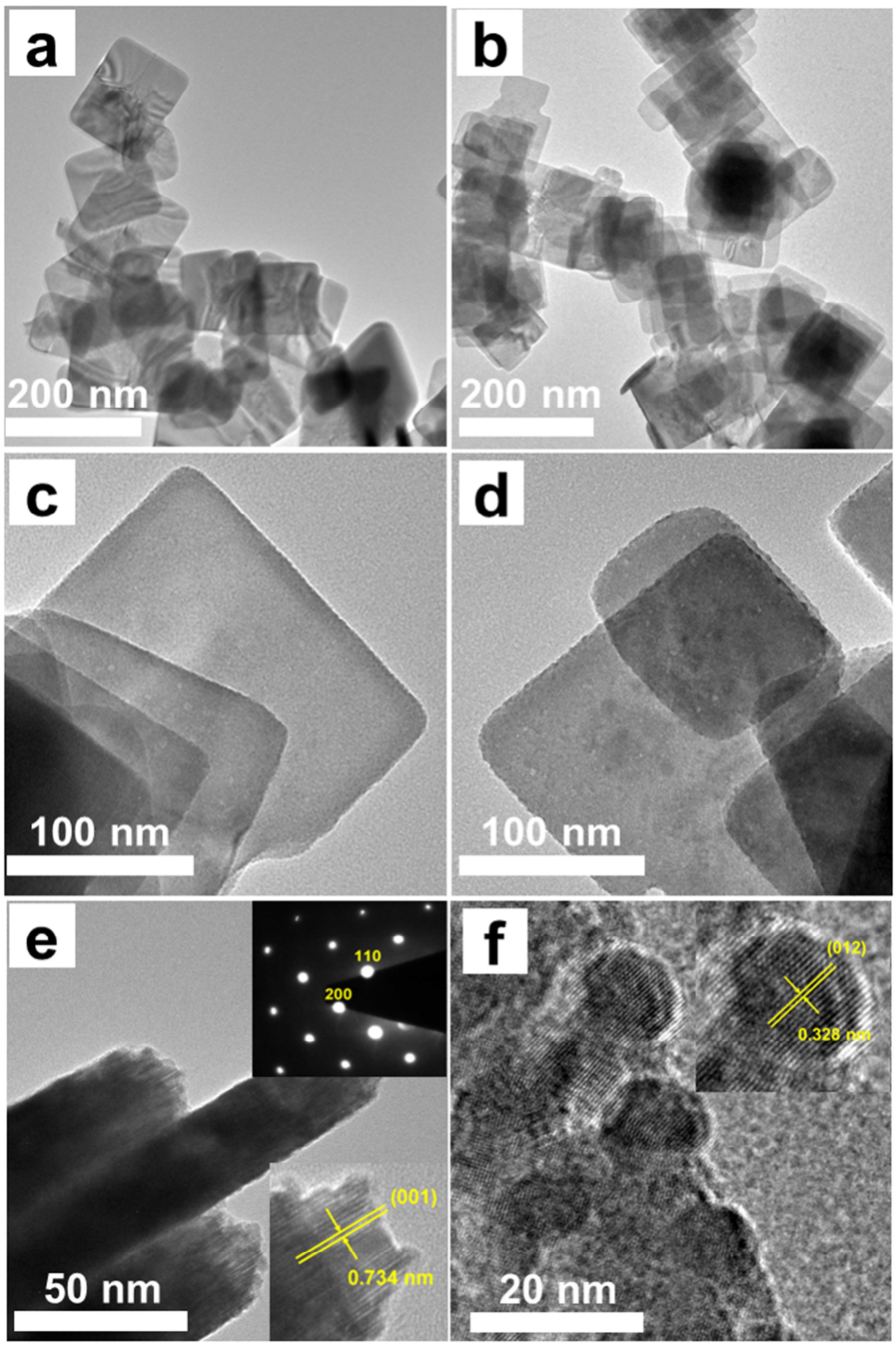
a
200 nm
b
200 nm
c
100 nm
d
100 nm
e
110
200
(001)
0.734 nm
50 nm
f
(012)
0.328 nm
20 nm

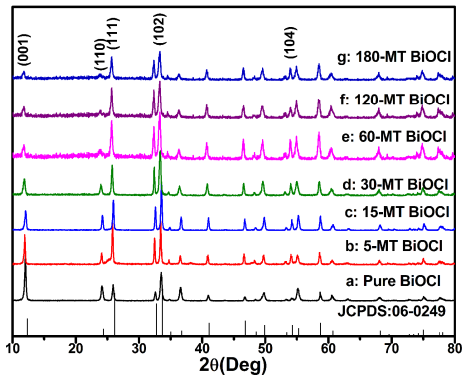

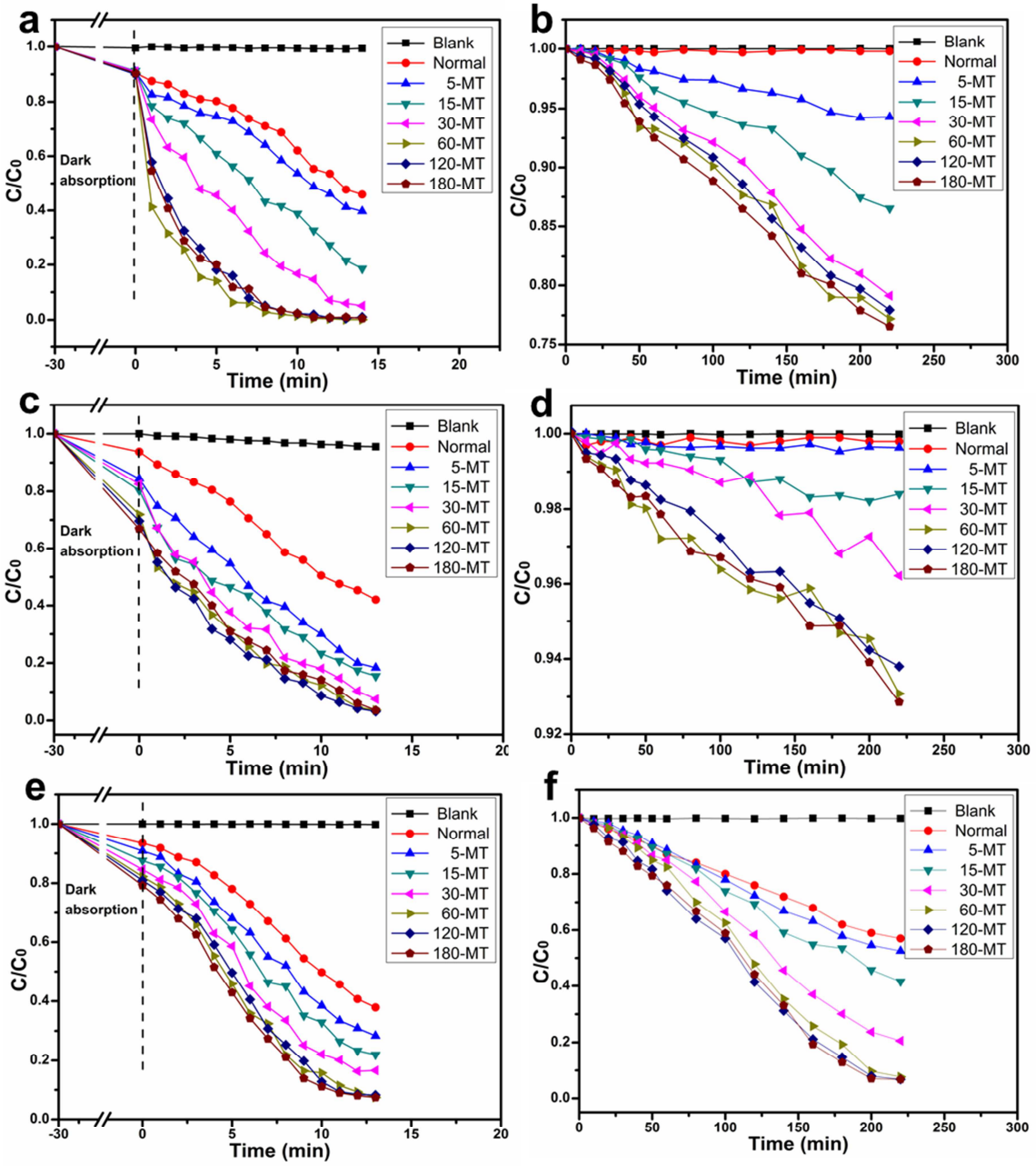
a
b
c
d
e
f
Blank
Normal
5-MT
15-MT
30-MT
60-MT
120-MT
180-MT
Dark absorption
C/C0
Time (min)

RhB:

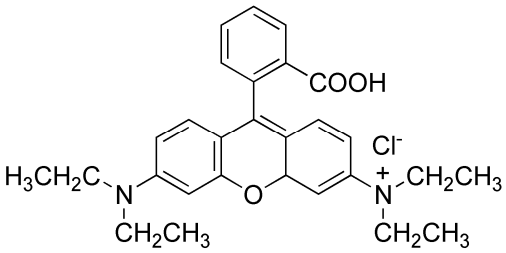

MO:

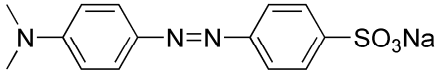

MB:

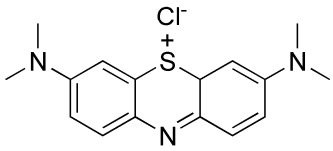

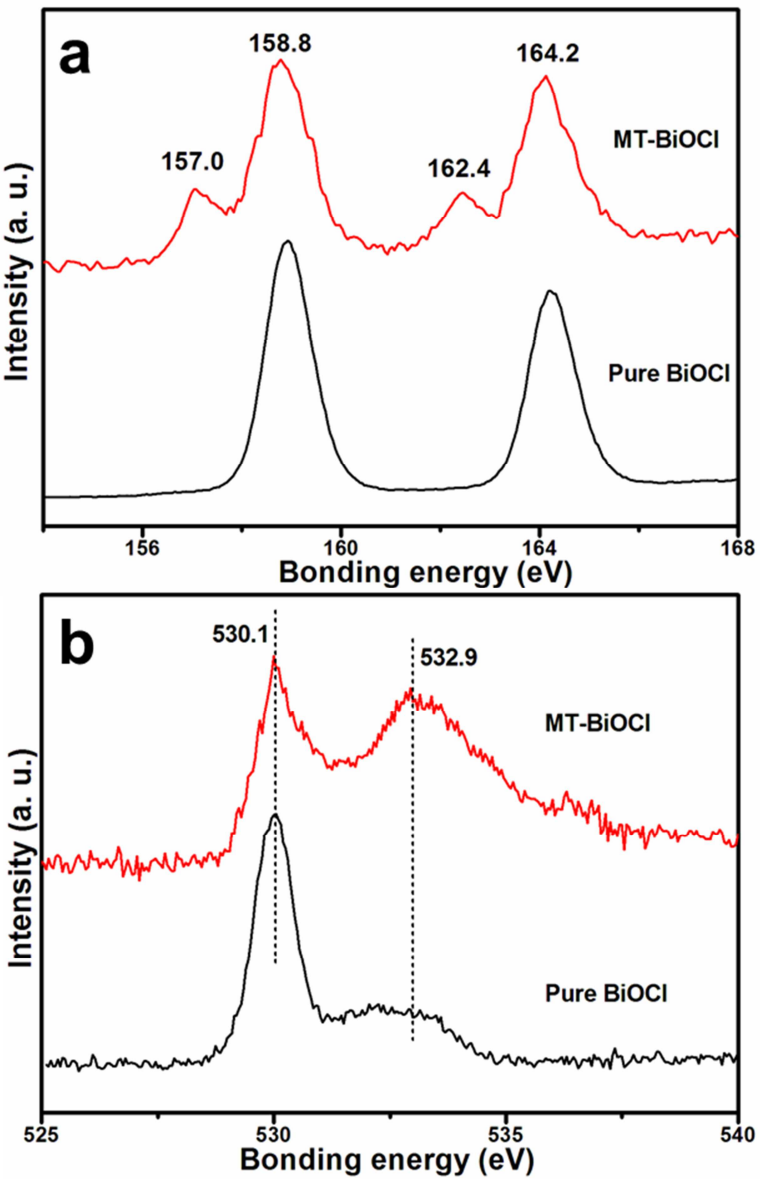
a
158.8
164.2
157.0
162.4
MT-BiOCl
Pure BiOCl
Intensity (a. u.)
156
160
164
168
Bonding energy (eV)
b
530.1
532.9
MT-BiOCl
Pure BiOCl
Intensity (a. u.)
525
530
535
540
Bonding energy (eV)

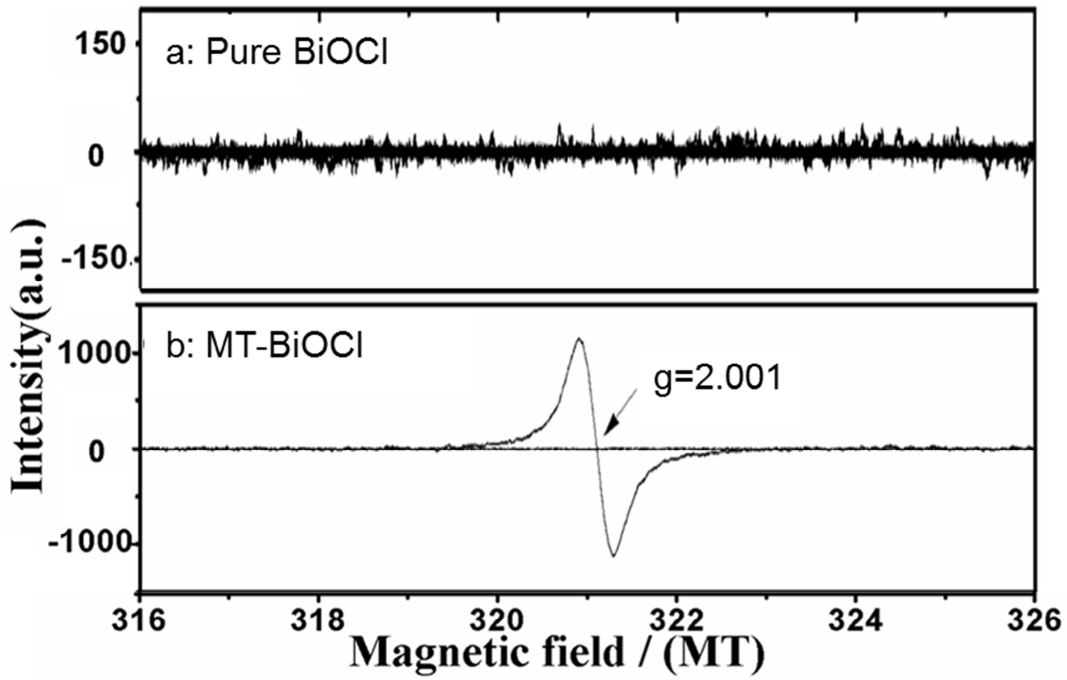

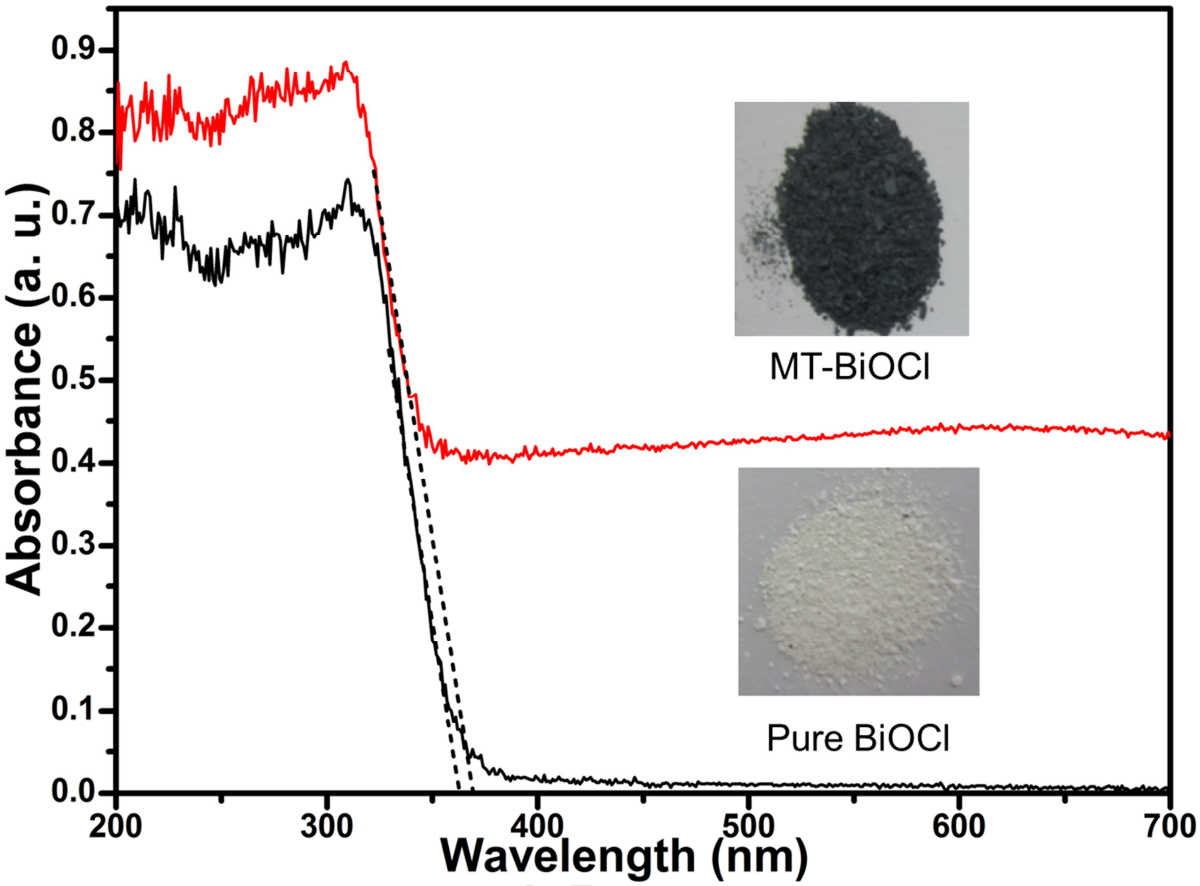
Absorbance (a. u.)
0.0
0.1
0.2
0.3
0.4
0.5
0.6
0.7
0.8
0.9
200
300
400
500
600
700
Wavelength (nm)
MT-BiOCl
Pure BiOCl

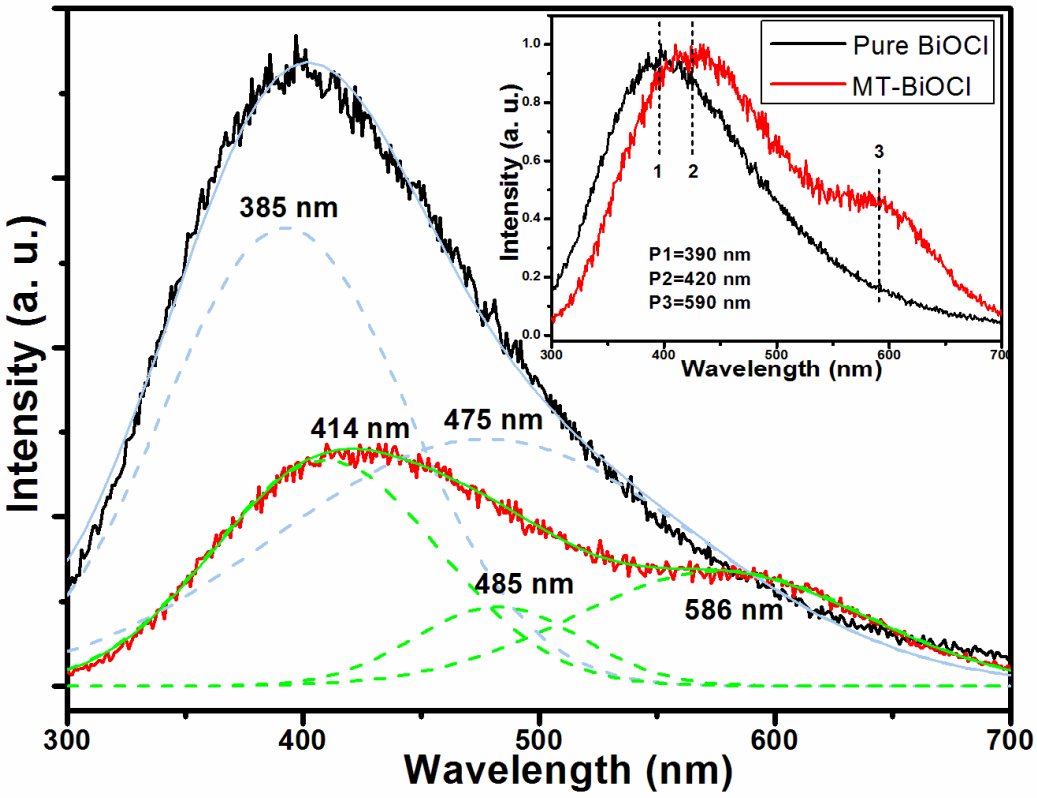
Intensity (a. u.)
Wavelength (nm)
385 nm
414 nm
475 nm
485 nm
586 nm
Pure BiOCl
MT-BiOCl
P1=390 nm
P2=420 nm
P3=590 nm
1
2
3

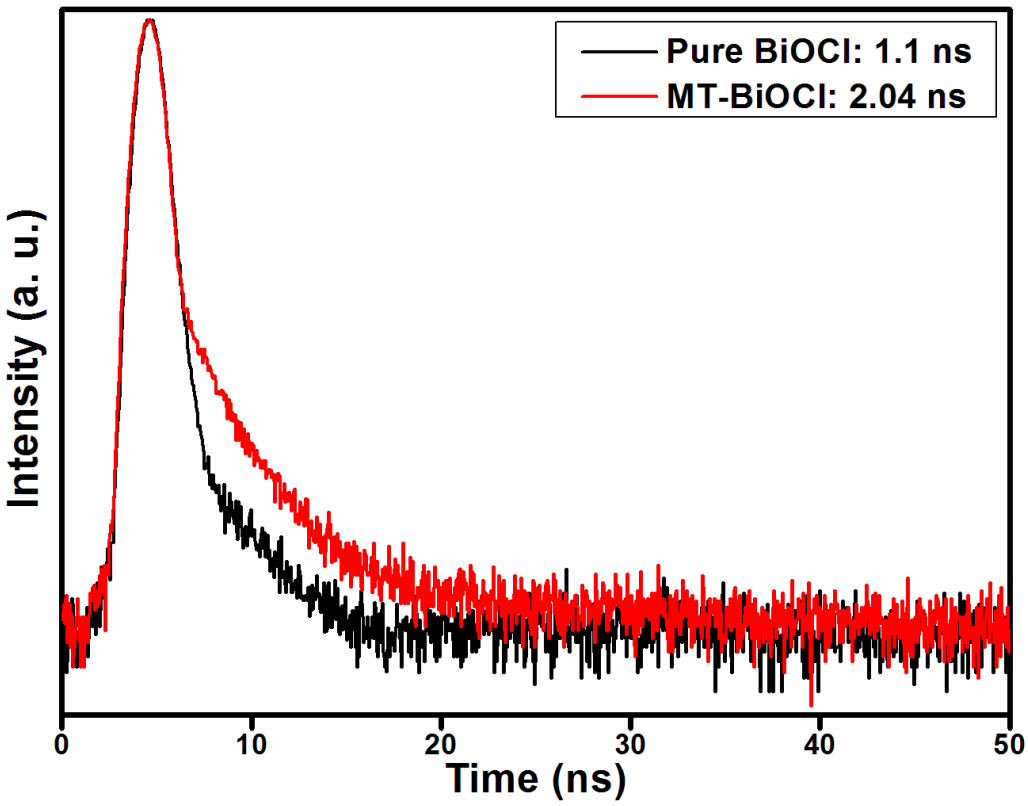
Pure BiOCl: 1.1 ns
MT-BiOCl: 2.04 ns
Intensity (a. u.)
0
10
20
30
40
50
Time (ns)

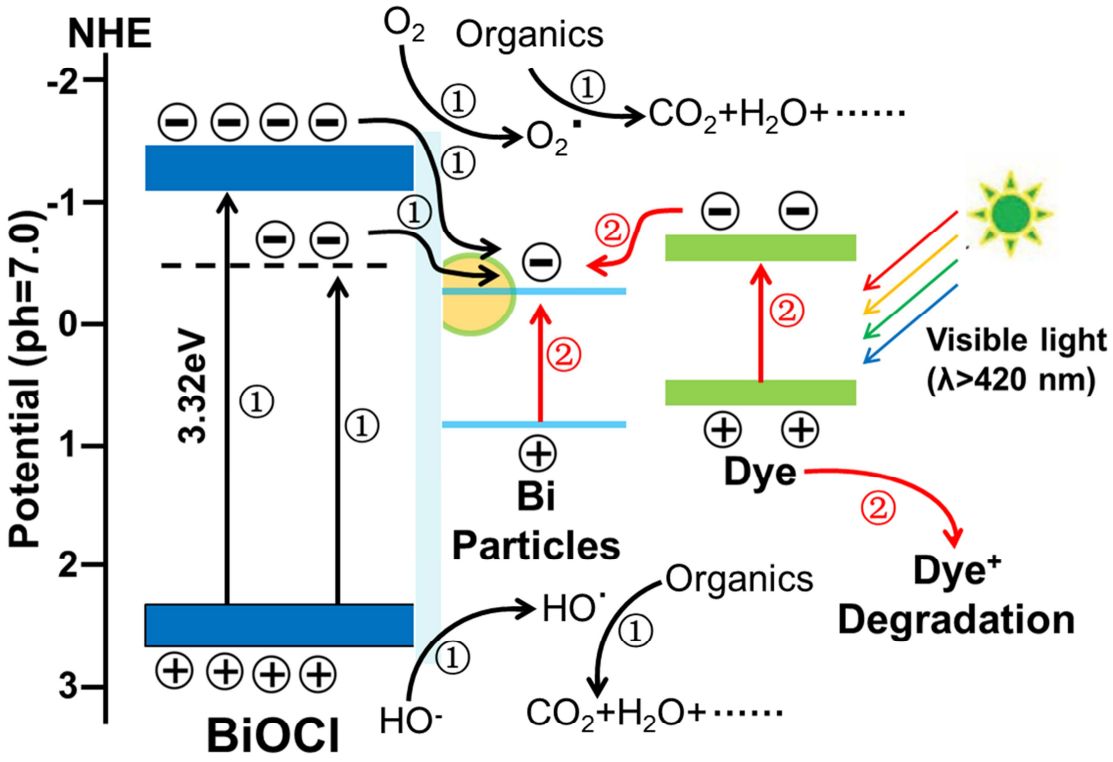

Research Highlight

1. Bi/BiOCl composites were synthesized via a microwave reduction.

2. Tunable selectivity photocatalytic activity can be achieved.

3. Photodegradation mechanism under UV and visible light were proposed.